Supplementary information: Intrinsically disordered nuclear pore proteins show ideal-polymer morphologies and dynamics

Luke K. Davis,[1,2,3] Ian J. Ford,[1,2] Anđela Šarić,[2,3,*] and Bart W. Hoogenboom[1,2,3,†]

[1] *London Centre for Nanotechnology, University College London, London WC1H OAH, United Kingdom*

[2] *Department of Physics and Astronomy, University College London, London WC1E 6BT, United Kingdom*

[3] *Institute for the Physics of Living Systems, University College London, London WC1E 6BT, United Kingdom*

[*] a.saric@ucl.ac.uk

[†] b.hoogenboom@ucl.ac.uk

METHODS

A. Molecular Dynamics (MD)

FG nups were modelled as polymers consisting of N identical beads with diameter d and bond length r_0, both set to 0.76 nm. Bonds were implemented using a harmonic potential $U_{bond}(r) = \frac{1}{2}k(r - r_0)^2$ with a spring constant $k = 500\ k_BT/\text{nm}^2$ where r is the distance between the centres of two beads.

To capture the steric repulsion between amino acids and the attraction/cohesion arising from hydrophobic effects, we imposed an excluded-volume and cohesive interaction between polymer beads [1]. The excluded-volume interaction is the Weeks-Chandler-Anderson (WCA) potential given by

$$U_{vol}(r) = \begin{cases} 4\epsilon_{LJ}\left[\left(\frac{\sigma}{r}\right)^{12} - \left(\frac{\sigma}{r}\right)^{6}\right] + \epsilon_{LJ}, & r \leq d, \\ 0, & d < r, \end{cases} \tag{1}$$

where $\epsilon_{LJ} = 500\ k_BT$ is the interaction strength and $\sigma = 2^{-\frac{1}{6}}d$; the addition of ϵ_{LJ} to the potential ensured that $U_{vol}(r = d) = 0.0\ k_BT$. The cohesive interaction is based on an infinitely ranged attractive pair potential

$$U(r) = \begin{cases} 0, & r < d, \\ -\epsilon_{pp}\exp\left(\frac{d-r}{\lambda}\right) & d \leq r, \end{cases} \tag{2}$$

where ϵ_{pp} is the cohesion strength and λ is the decay length [2]. We set $\lambda = 0.76$ nm and we imposed that no two beads interacted beyond the cutoff distance $r_c = 1.52$ nm, as it is not possible to have an infinitely-ranged potential in MD. In order to ensure the continuity of the pair potential at r_c we truncated and shifted the potential given by equation 2 using $U_{att}(r) = U(r) - U(r = r_c) - \left(\frac{dU(r)}{dr}\right)_{r=r_c}(r - r_c)$ [3] where $U_{att}(r)$ is the resulting cohesive pair potential given by

$$U_{att}(r) = -\frac{\epsilon_{pp}}{A}\left(\exp\left[1 - \frac{r}{d}\right]\left(1 - \frac{r(r - r_c)}{rd}\right) - \frac{1}{e}\right), \tag{3}$$

where e is Euler's number and $A = 1 + (d/l)^2 - 1/e$, where $l = 1.0$ nm is the unit of length. This ensured that the minimum of $U_{att}(r = d) = \epsilon_{pp}$. The total bead-bead pair potential,

$U_{pp}(r)$, with well depth ϵ_{pp} is given as

$$U_{pp}(r) = \begin{cases} U_{vol}(r) - \epsilon_{pp}, & r < d, \\ U_{att}(r), & d \leq r < r_c, \\ 0, & r_c \leq r, \end{cases} \tag{4}$$

where the minimum of $U_{vol}(r)$ is bought down to ϵ_{pp} to ensure continuity at $r = d$. MD simulations were performed using the LAMMPS package (2016) [4]. We subjected the polymer system to Langevin dynamics at a constant temperature, T, by implementing the NVE (constant number of beads N, constant volume V, constant total energy E) time integration algorithm in combination with a Langevin thermostat. We performed the simulations with dimensionless parameters with $T = 1$ and $\gamma = 1$, where γ is the friction coefficient, and a simulation timestep of $\delta t = 0.002$. To map simulation time to real time, we mapped one simulation timestep to 3.4×10^{-6} µs such that the self diffusion time of one bead in our model matched the self diffusion time of two attached amino acids (with size ≈ 0.76 nm) in water at room temperature, as outlined below. At least 34 µs were used to equilibrate the simulations, where equilibration was verified by inspection of the radius of gyration.

Mapping self diffusion times

To map the simulation timestep to a time scale relevant to real FG nups, we computed the diffusion coefficient, D, from simulations of 20 isolated beads (of radius $R = 0.38$ nm) and compared them with calculated diffusion constants for an alanine-proline dimer [5]. We fitted a straight line (with zero y-intercept) to the MSD which gave $D = (6.429 \pm 0.002 \text{ nm}^2)/6\Delta t$ where Δt is the unknown unit of time. We obtained the unit of time, Δt, via the Einstein-Stokes relation: $D = \frac{k_B T}{6\pi\eta R}$, where k_B is Boltzmann's constant, T is the temperature, η is the viscosity, and R is the radius of the bead. Using $k_B T = 4$ pNnm and $\eta = 8.90 \times 10^{-10}$ pNs/nm^2 for water at room temperature implied that the unit of time of the simulations was $\Delta t = 1.707 \times 10^{-9} s$. This produced a translational diffusion constant of $D = 0.627 \times 10^{-9}$ m^{2}s^{-1} for a bead which is comparable to diffusion constants calculated, from all-atom MD simulations with explicit solvent, for an alanine-proline dimer [5]. The elapsed simulation time is given by $t = N_s \times \delta t \times \Delta t$ where $\delta t = 0.002$ is the LAMMPS time step and N_s is the number of iterations for which a configuration of the system is recorded.

Single Polymer

To simulate an isolated polymer in the solvent we placed the first bead at the origin of a simulation box with side lengths of 600 nm. For these simulations a polymer started in an extended conformation where beads formed a straight line.

Polymer film

The first bead of each polymer was fixed to a vertex, $\mathbf{r}_\perp = (x_\perp, y_\perp, z_\perp = 0.0 \text{ nm})$, on a triangular lattice in the $x-y$ plane. We approximated a polymer film with infinite extension in the x and y directions through periodic boundary conditions. The hardness of the surface is implemented through a bead-surface interaction given by

$$U_{sur}(\Delta r_\perp) = \begin{cases} U_{vol}(\Delta r_\perp), & \Delta r_\perp < d, \\ 0, & \Delta r_\perp \geq d, \end{cases} \tag{5}$$

where $\Delta r_\perp$ is the distance between a bead to the nearest point on the surface passing through the tethering points. Polymers were grafted onto the surface at a density of 3.3 polymers per 100 nm^2, which is in the range of the grafting density of a yeast NPC that is thought to be 3.1 to 4.1 polymers per 100 nm^2 (i.e. 5.2 - 6.9 pmol per cm^2) [6]. The surface area was set to 545 nm^2 and 18 polymers were used. The initial condition was generated using a short MD simulation where polymer beads were attracted to the surface.

Polymer pore

We based the pore geometry on an NPC-mimetic system (NuPOD) that we have used previously [7]. In this system, 48 polymers were grafted onto freely rotating rods that were fixed on the inside of a stationary cylinder. The rods and cylinder consisted of beads and all polymer, rod, and cylinder beads interacted through excluded-volume interactions only. In addition, the beads of the polymers interacted through an attractive potential as outlined above (equation 4).

Calculating the dissociation constant

We calculated the dissociation constant K_D (in Molars) for two beads, in a simulation box with periodic boundary conditions, with cohesion strength ϵ_{pp}. We used the relation $K_D = K_A^{-1} = (N_A n_1 (V - V_D)/n_0)^{-1}$ [8], where K_A is the association constant, N_A is Avogadro's number, n_1 is the number of simulation trajectories containing two beads that form a dimer, *i.e.*, the inter-particle separation is $\leq r_D$ where r_D is the dimerization cut-off, V is the volume of the simulation box ((6 nm)^3), $V_D = 4\pi r_D^3/3$ is the dimerization volume of one bead (with a volume, excluding the dimerization volume, per bead $(V - 2V_D)/2$ of 106-108 nm^3 for r_D between 0.76-0.38 nm respectively [8]), and n_0 is the number of simulation trajectories containing two beads that have an inter-particle separation $> r_D$.

Model parameterization

To set the cohesion strength ϵ_{pp} for polymers with lengths corresponding to FG nups (Table S1) we performed MD simulations of single polymers with $\epsilon_{pp} = (0.0, 0.2, 0.4, 0.6, 0.8, 1.0)$ k_BT. We computed the ensemble averaged Stokes radius R_S, the radius of a sphere that has the same diffusion coefficient as the polymer, from simulations run for 68 µs, using the HYDRO++ program (version 10) [9] assuming a temperature of 20.0 ℃, a solvent viscosity of 0.01 gcm^{-1}s^{-1}, and solution density of 1.0 g/cm^3. In order to find the ϵ_{pp} for a particular FG nup in this model, we interpolated the calculated Stokes radii as a function of ϵ_{pp} and solved for the ϵ_{pp} that yielded the experimental Stokes radius.

Model validation

To validate the parameterized polymer model we simulated polymer films at cohesion strengths ϵ_{pp} =(0.0, 0.2, 0.4, 0.6, 0.8, 1.0) k_BT and calculated the model film thickness predictions by numerically solving $\int_0^{z_\kappa} \rho(z)dz / \int_0^{\infty} \rho(z)dz = \kappa$, where κ is the chosen fraction of beads and z_κ is the distance above the surface that contains $\kappa N_p N$ beads. The film thickness is calculated with $\kappa = 0.95 \pm 0.05$, similar to previous comparisons between computational and experimental data [6]. The max height used for the density profile was 250 nm with 0.5 nm/bin for the histogramming. To obtain the film thickness at the NPC grafting density from the experimental data, we first fitted datasets, for a range of grafting densities,

to a function $Z(D) = AD^B$, where Z is the thickness, D is the grafting distance between polymers, and $\{A, B\}$ are fitting parameters. We assumed that the average film thickness goes to zero for $D \gg 1$ nm. The experimental film thickness at the NPC grafting distance is then defined as $Z(D_H)$ where $D_H = \sqrt{\frac{1.15 \cdot 10^3}{6g}}$ is the grafting distance, $g = 5.4$ pmol/cm^2 is the approximate NPC grafting density, and the numerical factors convert g to a grafting distance on a triangular lattice in units of nm.

File compressibility

To quantitatively compare polymer film and pore assemblies, we used a measure of bead compaction that could be implemented in the same way irrespective of geometry. We used the file compressibilty quantity which represents how much a data file containing bead coordinates can be losslessly compressed [10]. To compute the file compressibility we first calculated the minimum volume of a box, V_0, that contained all polymer beads in a system with $\epsilon_{pp} = 0.0\ k_BT$. V_0 was then discretized into cubes with side length $l = 0.76$ nm. For a simulation run at a certain ϵ_{pp}, every 0.34 µs the simulation box was raster scanned to check if a cube was inside a bead (= 1) or not (= 0), and a file was generated containing all the states of the cubes. These files were then losslessly compressed using the bzip2 facility [11] and the average of the file sizes, $\varrho_{ave}(\epsilon_{pp})$, were computed. The file compressibility parameter was defined as $\varrho = (\varrho_{ave}(\epsilon_{pp}) - \varrho_{min})/(\varrho_{ave}(0.0) - \varrho_{min})$, where ϱ_{min} is a reference compressed file size of a maximally ordered file containing a sequence of 0s only. For all cases the total number of characters in the uncompressed state file was V_0/l^3.

Resealing simulations

To investigate the parameterized model in a dynamic setting, we investigated the dynamic behaviour of polymer pore assemblies by performing 'resealing' simulations, where a hole (void of polymer beads) with diameter d_{hole} is artificially made at the centre of the polymer-coated pore and 'resealing' begins when this constraint is removed. The initial hole was created through a simulation where a cylinder with radius $d_{hole}/2$ and length $L = 200$ nm was dragged through the polymers inside the pore. The cylinder was a continuum, *i.e.*, not constructed of point like beads, and the distance between a bead and the cylinder was

defined as the distance from the bead to the nearest point on the surface, therefore the force the surface exerted on the bead was along the direction that is normal to the surface at that point. The cylinder was placed at an initial height so as not to make contact with any bead, and with its axis permanently aligned with the pore scaffold. The centre of the cylinder was then incrementally moved towards the origin. The cylinder and beads interacted through excluded-volume only using the WCA pair potential given by equation 1. Whilst the cylinder was moving an external constraint was imposed to force polymer beads to within the axial dimensions of the pore scaffold, without causing overlapping between beads. The simulation imposing the constraints was run for 0.34 µs and then a second simulation, marking the beginning of resealing, was performed with the cylinder and external constraints removed. The resealing of the pore is quantified through a central density, *i.e.*, the number of beads in a circle of radius 5 nm located at the origin, which we compute every 0.34 µs, and we fit this data to a relaxation function $\rho(t) = \rho_0 \left(1 - \exp\left(-t/\tau\right)\right)$, where ρ is the central density, ρ_0 the equilibrium central density, t is time, and τ is the resealing time: the time taken for the central density to reach $\approx 0.63\rho_0$.

B. Density Functional Theory (DFT)

To investigate molecular interactions in a polymer system we have used classical density functional theory (DFT), a scheme based upon the minimisation of a dimensionless free energy functional $\mathcal{F}$ that depends solely on the number density of beads $\rho(r)$, and is written as $\mathcal{F}[\rho(r)]$ [12]. In this work we have formulated DFT using mean-field theory so that the many-body polymer interactions are reduced to a single polymer interacting with a dimensionless mean field $w(r)$. The optimum mean field minimizes $\mathcal{F}$ and produces as output the equilibrium number density.

To model planar assemblies of FG nups, we formulated a 1D version of a previously successful 2D DFT formulation [6], where polymers were grafted onto the base of a cylinder with the assumption of rotational symmetry along the axial coordinate. This DFT has been previously described in extensive detail [2, 6, 13]. Here we describe the 1D version, consisting of polymers grafted onto a flat surface and assuming translational symmetry along this surface. The determining coordinate was therefore the height z above the grafting surface.

We took the approximation $\mathcal{F} = \mathcal{F}_0 + \{\mathcal{F}_{vol} + \mathcal{F}_{att} + \mathcal{F}_{sur} + \mathcal{F}_{mf}\}$ where $\mathcal{F}_0$ is the free

energy functional describing a chain of N non-interacting point-like beads in the mean field, and excess terms representing excluded-volume, attractive, surface, and compensating mean field interactions respectively. $\mathcal{F}_0$ is defined by the Hamiltonian

$$H_0 = \sum_{i=0}^{N-1} h(r_{i+1}, r_i) + k_B T \sum_{i=1}^{N} w(z_i), \tag{6}$$

where h is a function (and r is the magnitude of bead separation) that imposes a rigid bond length of r_0 between beads in a chain and $w(z)$ is the 1D mean field.

$\mathcal{F}_{vol}$ is the free energy functional imposing the excluded volume interactions between beads. To impose the excluded volume interactions, we used fundamental measure theory

$$\mathcal{F}_{vol} = \int (\phi_{wb} + \phi_{ch})\, dz, \tag{7}$$

where ϕ_{wb} is the white bear functional [14] and ϕ_{ch} is the chain connectivity functional [15]. ϕ_{wb} is given by

$$\phi_{wb} = -\, n_0 \log(1 - n_3) + \frac{n_1 n_2 - \overline{n}_1 \cdot \overline{n}_2}{1 - n_3} + (n_2^3 - 3 n_2 \overline{n}_2^2) \frac{n_3 + (1 - n_3)^2 \log(1 - n_3)}{36 \pi n_3^2 (1 - n3)^2} \tag{8}$$

and ϕ_{ch} is

$$\phi_{ch} = \left(\frac{1 - N}{N} \right) n_0 \left(1 - \frac{\overline{n}_2^2}{n_2^2} \right) \log \left(\frac{1}{1 - n_3} + \frac{n_2 R \left(1 - \frac{\overline{n}_2^2}{n_2^2} \right)}{2 \left(1 - n_3 \right)^2} + \frac{n_2 R^2 \left(1 - \frac{\overline{n}_2^2}{n_2^2} \right)}{18 \left(1 - n_3 \right)^3} \right), \tag{9}$$

where $R = d/2$ is the bead radius and $\{n_\alpha\}$ and $\{\overline{n}_\alpha\}$ are sets of scalar and vector weighted densities, respectively, that are given by

$$n_\alpha(z) = \int \rho(z') \omega_\alpha(z - z') dz, \qquad \alpha = 0, 1, 2, 3, \tag{10a}$$

$$\overline{n}_\alpha(z) = \int \rho(z') \overline{\omega}_\alpha(z - z') dz, \qquad \alpha = 1, 2, \tag{10b}$$

where $\rho(z)$ is the one dimensional number density, ω_α and $\overline{\omega}_\alpha$ are the 1D geometrical weight functions of a sphere [16] given as $w_2(z) = 2\pi R \theta(R - |z|)$, $\overline{w}_2(z) = 2\pi z \overline{e}_z \theta(R - |z|)$, $w_3(z) = \pi(R^2 - z^2)\theta(R - |z|)$, $w_1(z) = w_2(z)/(4\pi R)$, $\overline{w}_1(z) = \overline{w}_2(z)/(4\pi R)$, $w_0(z) = w_2(z)/(4\pi R^2)$, where $\overline{e}_z$ is a unit vector and θ is the Heaviside function.

The cohesive term in the free energy, $\mathcal{F}_{att}$, is implemented using the random phase approximation [17] and is given by

$$\mathcal{F}_{att} = \frac{\beta}{2} \int \int \rho(z') \rho(z) U_{att}^{\perp}(z - z') dz dz', \tag{11}$$

where $\beta = 1/k_BT$ and $U_{att}^{\perp}(z) = \int_{-\infty}^{\infty}\int_{-\infty}^{\infty} U_{att}(r)dxdy$ (integrated over an infinite grafting area) with r being the magnitude of vector separation between beads, and U_{att} is given by equation 3.

The free energy term representing the interactions between beads and the surface is given as

$$\mathcal{F}_{sur} = \beta \int \rho(z) U_{sur}(z) dz, \tag{12}$$

with U_{sur} as given in equation 5. The mean field energy, $\mathcal{F}_{mf}$, is the dimensionless free energy term that compensates for the introduction of a mean field and is given as

$$\mathcal{F}_{mf} = \int w(z)\rho(z)dz, \tag{13}$$

To incorporate a number of polymers, N_p, one multiplies $\mathcal{F}_0$ by N_p and interprets $\rho(z)$ as the number density of N_pN beads. To compute $\rho(z)$, we solved the 1D diffusion equation for a random walk with contour length Nr_0 in the presence of an external field $w(z)$ [2]. We optimized $w(z)$ through a discrete update rule

$$w_{n+1}(z_j) = w_n(z_j) + \Delta t \left(-w_n(z_j) + \mu_n(z_j) + \beta \sum_i^M \rho_n(z_i) U_{att}^{\perp}(z_i - z_j)\Delta z + \beta U_{sur}(z_j) \right), \tag{14}$$

where n is an index representing the current iteration, Δt is the update timestep, $\{i, j\}$ are labels denoting discrete space, μ is the functional derivative of $\mathcal{F}_{vol}$ with respect to $\rho(z)$, and M is the total number of discrete spatial points (along the z axis). To ensure the stability of the update rule we used M= 1024 and $\Delta z = z_{max}/M$ (z_{max} = 100 nm so that polymer beads were well within the spatial domain), Δt= 0.001, and the initial mean field was set to zero for all z. Convergence was obtained when $w_{n+1}(z_j) - w_n(z_j) \leq 10^{-7}$ for all j.

Calculating the second virial coefficient

We considered two beads, treated as weakly attractive ($\epsilon_{pp} \leq k_BT$) hard spheres, interacting with a pair potential given by equation 4. The second virial coefficient, $B_2(\epsilon_{pp})$, is given as

$$\begin{aligned} B_2(\epsilon_{pp}) &= 2\pi \left(b + \int_{r_0}^{r_c} r^2 \left(1 - \exp\left(-U_{att}(r)/k_BT\right)\right) dr \right), \\ &\approx 2\pi \left(b + \int_{r_0}^{r_c} r^2 \frac{U_{att}(r)}{k_BT} dr \right), \end{aligned} \tag{15}$$

where $b = r_0^3/3$, $r_0 = d$ is the contact distance between two beads, and r_c is the cut-off of the attractive potential ($= \infty$ for infinite ranged potentials) [18].

SUPPLEMENTARY TABLES AND FIGURES

FG nup	No. of amino acids	Protein volume (nm^3) [a]	Polymer volume (nm^3) [b]	Charged /hydrophobic ratio [c]	Single polymer		Polymer film		Source
					R_S (nm)	ϵ_{pp} (kT)	Thickness (nm)	ϵ_{pp} (kT)	
Nsp1	95	9.1	10.8	1.31	2.68	0.50	-	-	[20]
Nsp1p-5FF	150	15.3	17.0	1.27	4.4	- [d]	5.68	0.54	[21]
Nup60	151	15.3	17.2	0.95	3.13	0.47	-	-	[20]
Nsp1n	172	15.2	19.7	0.08	2.71	0.69	-	-	[20]
Nup100s	190	19.3	21.72	1.0	3.66	0.42	-	-	[20]
Nup145Ns	191	19.4	21.8	0.89	2.98	0.60	-	-	[20]
Nup116s	196	20.7	22.4	1.35	3.91	0.36	-	-	[20]
Nup42	212	18.5	24.3	0.14	2.84	0.72	-	-	[20]
Nup49	215	18.4	24.6	0.13	2.69	0.93	-	-	[20]
Nup62	240	20.5	27.5	0.03	3.7	0.49	4.62	0.91	[22]
Nup145N	242	21.7	27.7	0.14	2.82	0.85	-	-	[20]
Nup57	255	22.3	29.2	0.14	3.19	0.61	-	-	[20]
Nup1c	279	24.8	31.9	0.14	3.24	0.63	-	-	[20]
Nup214	282	23.8	32.3	0.14	3.4	0.60	2.64	1.10	[22]
Nsp1p-12FF	283	27.9	32.3	1.4	4.3	0.42	9.03	0.47	[21]
Reg-FSFG	315	27.8	36.4	0.0	-	-	11.01	0.44	[6]
Nup2	376	36.7	43.0	1.1	5.98	0.15	-	-	[20]
Nsp1m	431	40.9	49.4	1.22	6.53	0.19	-	-	[20]
Nup159	441	40.6	50.6	0.69	5.54	0.40	-	-	[20]
Nup98-Glyco	496	45.1	56.9	0.2	-	-	16.22	0.41	[6]
Nup98	498	44.7	57.1	0.2	5.6	0.40	5.24	0.72	[22]
Nup116m	551	48.9	63.2	0.11	4.65	0.50	-	-	[20]
Nup1m	578	57.0	66.3	1.08	6.79	0.38	-	-	[20]
Nup153	602	55.7	69.1	0.5	5.1	0.48	10.31	0.50	[22]
Nup100n	609	54.9	69.9	0.11	4.87	0.49	-	-	[20]
Nsp1	615	57.4	70.4	0.93	-	-	27.09	0.34	[6]
Nup2p	720	72.1	82.6	1.11	7.9	0.28	-	-	[23]

[a] Sum of Van der Waals volumes for each specific amino acid [19].

[b] Sum of bead volumes. A diameter of 0.76 nm is used for all calculations.

[c] Based on the same amino acid classification as used in [20].

[d] Experimental Stokes radius is slightly overestimated due to polydispersity [21].

TABLE S1. Characterisation, and experimental dimensions (Stokes radius R_S and film thickness), of the resulting cohesion strengths (ϵ_{pp}, from MD) for all FG nups used in this work.

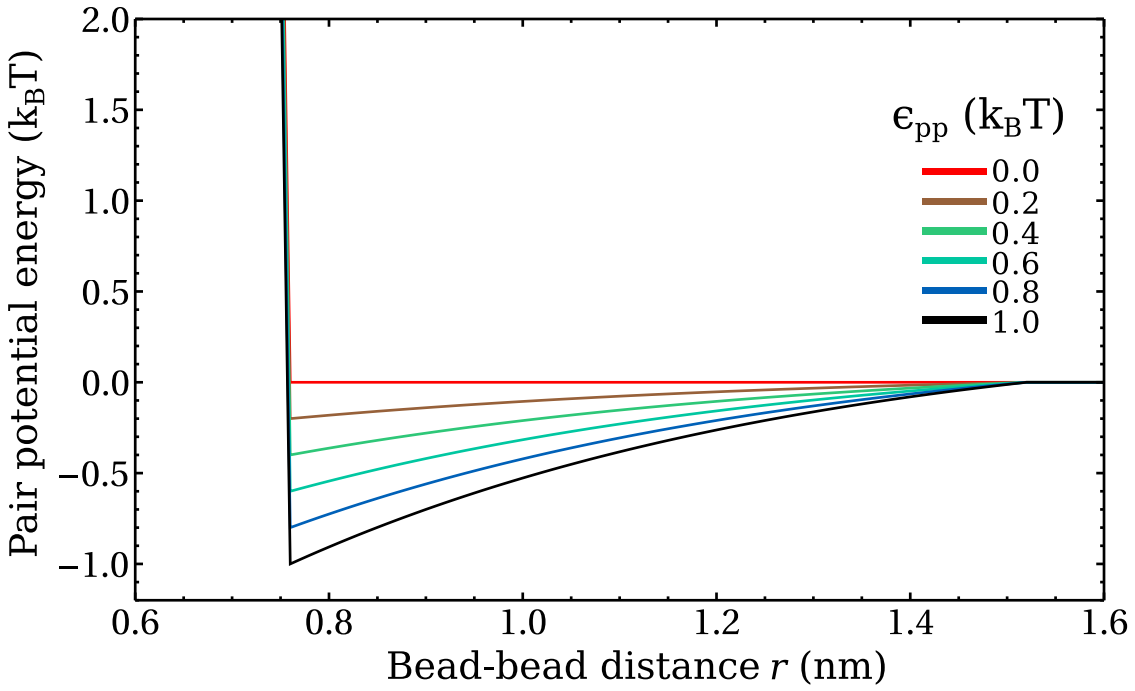

FIG. S1. Defining and quantifying the interactions between polymer beads. **a)** Plot of the total pair potential energy, $U_{pp}(r)$, between two polymer beads, with a diameter of 0.76 nm, at a centre-to-centre distance r, shown for various cohesion strengths ϵ_{pp}. **b)** The dissociation constant K_D between two individual polymer beads as a function of ϵ_{pp}, for three choices of the dimerization cut-off (see Methods): the maximum inter-particle separation at which two beads are considered a dimer. For all choices of the dimerization cut-off, the number of simulation trajectories containing dimers was > 2000.

Interaction regime	$R_S = A_0(N_{AA})^\nu$		$R_G = A_0(N_{AA})^\nu$	
	A_0 (nm)	ν	A_0 (nm)	ν
$\epsilon_{pp} = 0.0\ k_BT$	0.26 ± 0.02	0.55 ± 0.01	0.22 ± 0.05	0.61 ± 0.03
$\epsilon_{pp} = \langle\epsilon_{pp}\rangle_{FG}$	0.47 ± 0.04	0.38 ± 0.02	0.4 ± 0.1	0.38 ± 0.04
$\epsilon_{pp} = 1.0\ k_BT$	0.63 ± 0.05	0.27 ± 0.01	0.54 ± 0.05	0.24 ± 0.02
Ideal	0.35 ± 0.03	0.42 ± 0.01	0.25 ± 0.04	0.48 ± 0.03
Experiment	0.2 ± 0.3	0.5 ± 0.2	-	-

TABLE S2. Fitting parameters for R_S and R_G using a power law fit, where N_{AA} is the number of amino acids. Note that the obtained values of the scaling exponent ν do depend on the choice of A_0 (here left as a free fitting parameter). The uncertainties represent 95% confidence intervals.

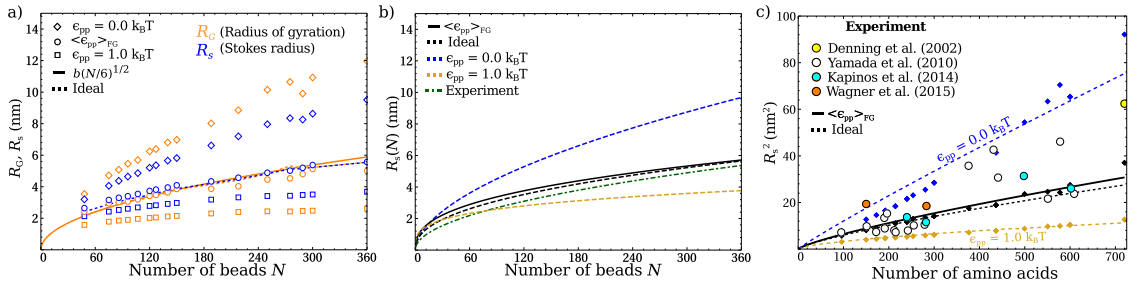

FIG. S2. Further quantification of single-molecule morphologies. **a)** Comparing the Stokes radii R_S to the radius of gyration R_G for various interaction regimes as calculated from MD simulations of polymers with a bead diameter of 0.76 nm. **b)** Comparing Stokes radii from MD simulations to experiments, as in Figure **??**c but here using a bead diameter of 0.57 nm, *i.e.*, a polymer with a predicted persistence length smaller than that for FG nups (0.29 nm) and with an excluded volume that underestimates that of FG nups by $\approx 30\%$. The beads interacted through an attractive pair potential, as given in equation 3, with d=0.57 nm and with a cut-off range $r_c = 1.52$ nm. In this model $\langle \epsilon_{pp} \rangle_{FG} = 0.21 \pm 0.06\ k_BT$. As for the model discussed in the main text, the behaviour for this $\langle \epsilon_{pp} \rangle_{FG}$ closely matched the predictions for ideal polymers.

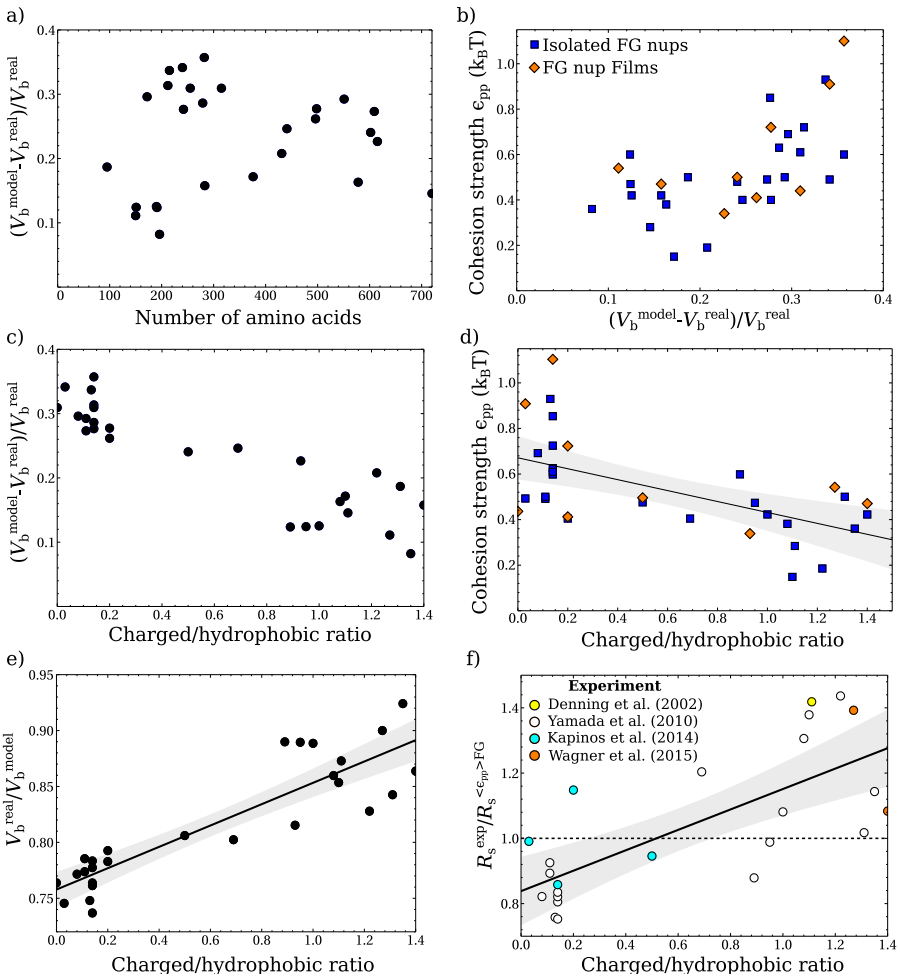

FIG. S3. Model dependence on overestimates of the excluded volume for different FG nups. **a)** The fractional overestimation of the excluded volume of an FG nup (V_b^{real}), *i.e.*, the total sum of the Van der Waals volumes, by the excluded volume of a polymer in the model (V_b^{model}), *i.e.*, the total sum of the bead volumes. **b)** For FG nups that have a smaller total amino acid volume compared with the polymer model (*i.e.*, for which the excluded-volume is overestimated by a larger amount in our model), a larger effective ϵ_{pp} is needed to describe the (more compact) morphology of those FG nups. **c,d)** In line with previous work [20], we can classify the different FG nups according to their relative contents in terms of more charged and more hydrophobic amino acids and note that both the fractional overestimation of the excluded volume and the cohesion strength ϵ_{pp} follow the same trend. **e,f)** Both the overestimation of the excluded volume and the experimental Stokes radii (relative to the prediction of $\langle\epsilon_{pp}\rangle$) show the same trend as a function of the ratio of charged and hydrophobic amino acid contents of the FG nups. This suggests that such variations between FG nups are simply do to differences in their excluded volume, and not to systematic differences in charge/hydrophobicity as proposed previously [20].

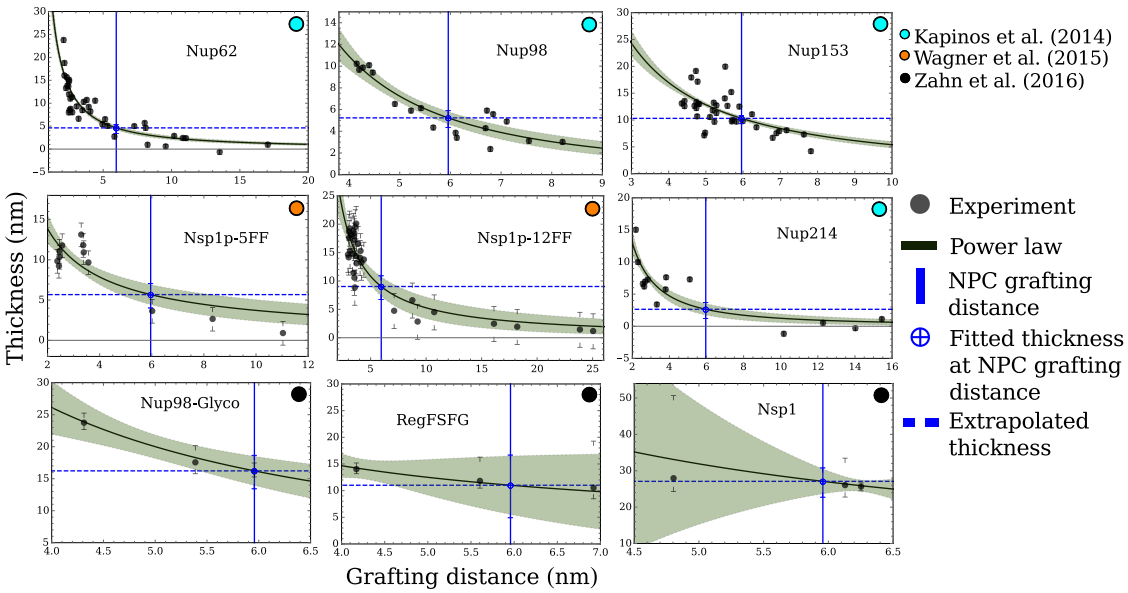

FIG. S4. Interpolation of the experimental data from FG nup films, to estimate the film thickness for a grafting distance/density that corresponds to the NPC (3.2 polymers/100 nm^2, or 5.4 $pmol/cm^2$). Data were fitted with a power law, with 95% mean prediction bands (green shading).

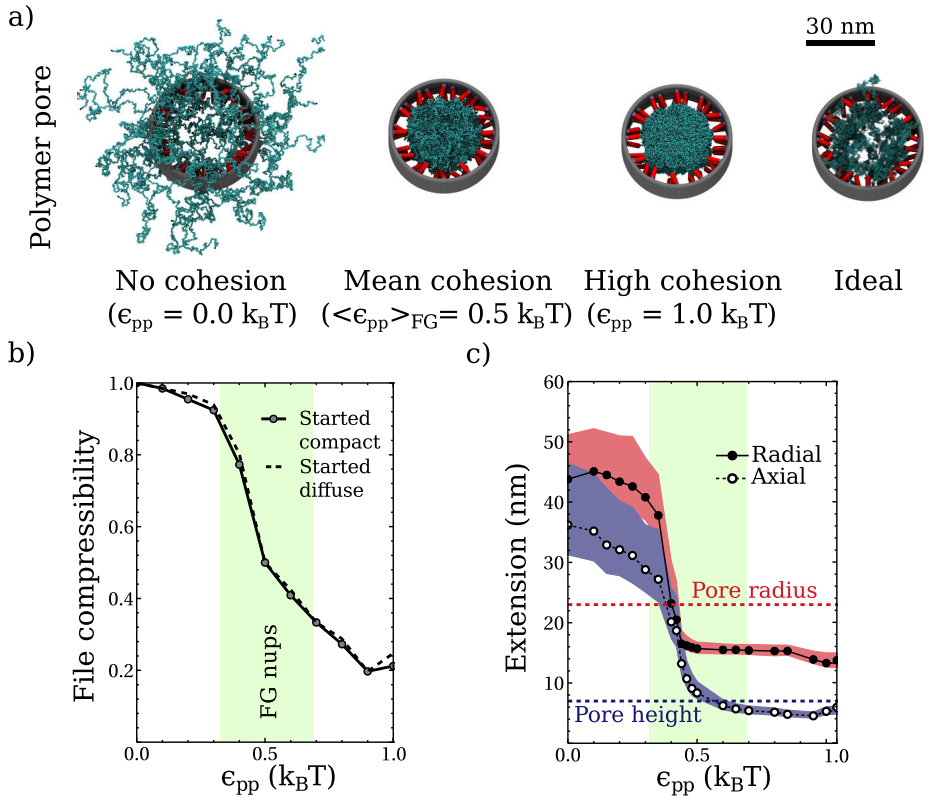

FIG. S5. Morphologies for polymers grafted inside an NPC-mimicking nanopore [7]. **a)** MD equilibrated snapshots of polymers in a pore for various interaction regimes (N_p = 48 polymers, N = 300 beads). Polymers are shown in blue; the inner diameter of the (DNA origami) pore scaffold is shown in grey; and conjugated DNA handles (freely rotating, rigid rods) in red. **b)** A measure of polymer compaction, file compressibility, is plotted as a function of ϵ_{pp} for the different starting conditions of the simulations. **c)** Polymer extension in the pore as a function of ϵ_{pp}. The red band denotes the upper and lower radial extension thresholds that represent the radial distance from the centre containing 99% and 90% of the total bead count respectively; the purple band refers to the axial extension.

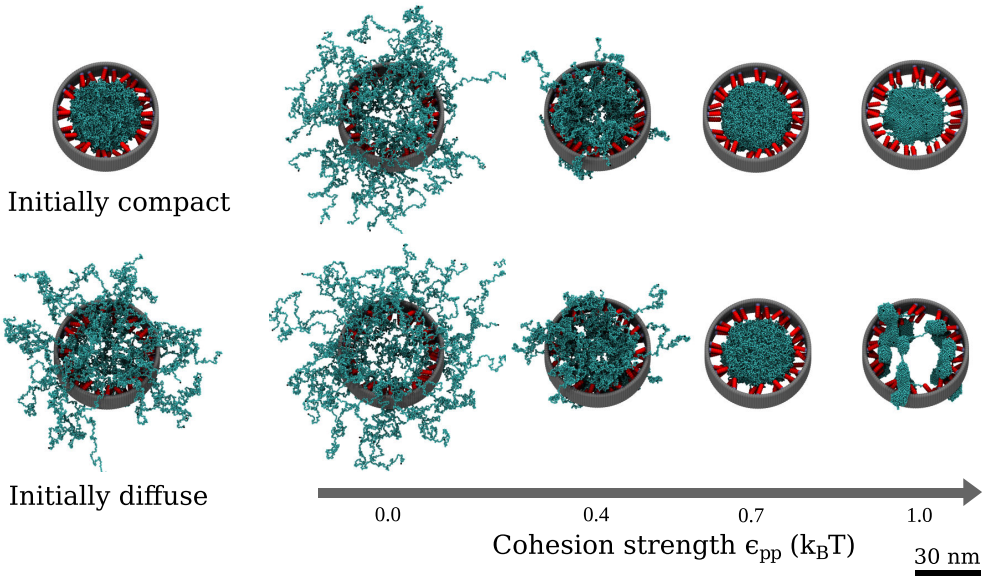

FIG. S6. Snapshots of polymer pore configurations (see Figure S5) for various ϵ_{pp} from two different initial conditions.

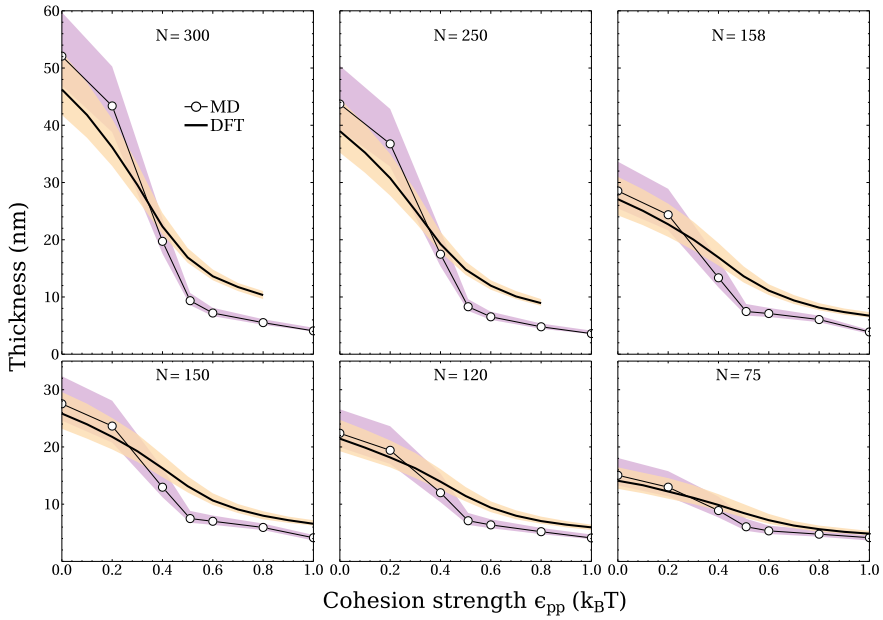

FIG. S7. Benchmarking DFT against MD film data for the thickness of FG nup films, as a function of cohesion strength ϵ_{pp}. The bands denote a tolerance of $\pm 5\%$ of the total number of beads. DFT thicknesses at $\epsilon_{pp} > 0.8\ k_BT$ were unavailable for $N = 250$ and 300 beads, since the dense packing complicated the convergence of the DFT calculations.

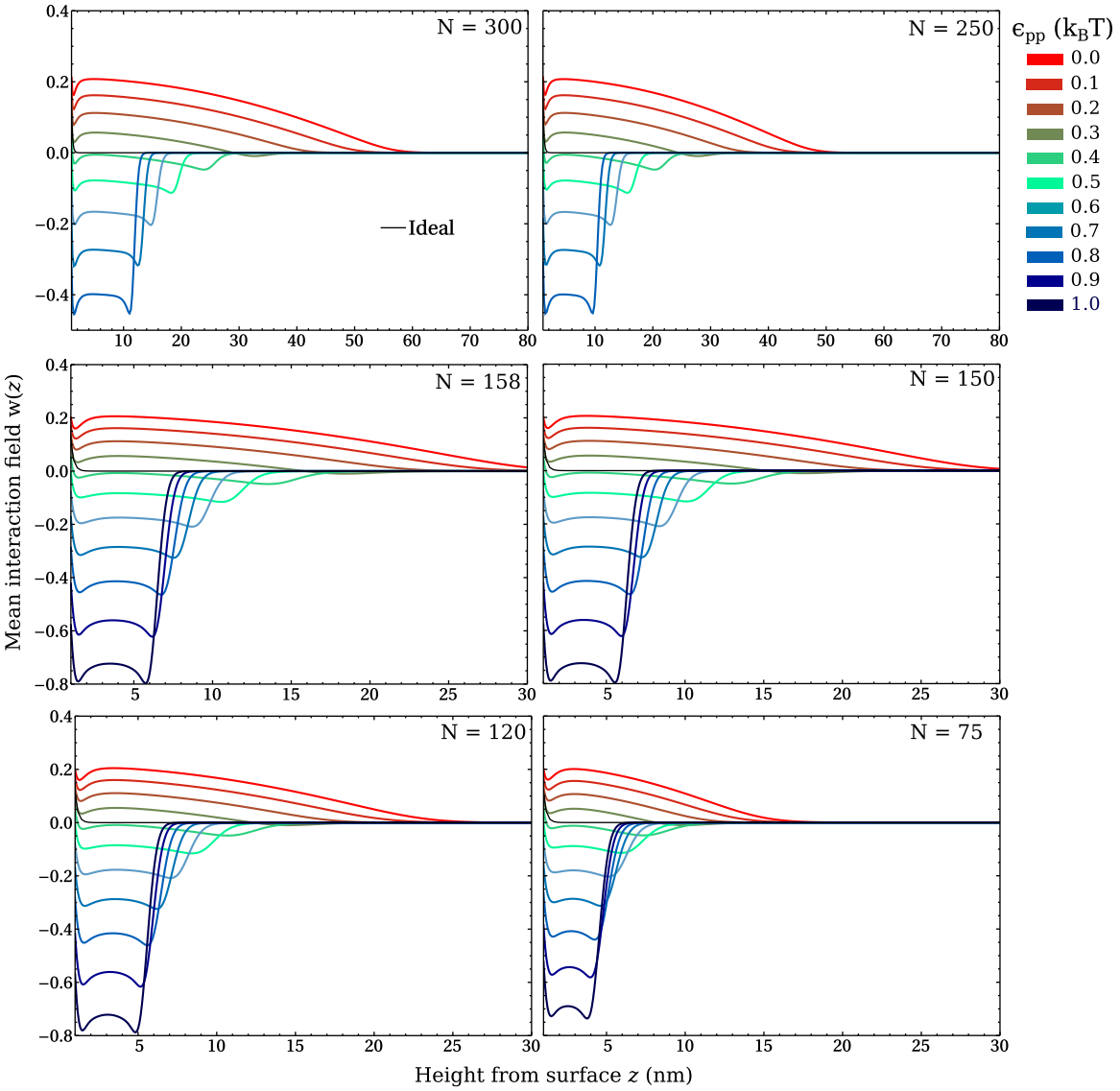

FIG. S8. DFT equilibrium mean fields $w(z)$ (see equation 6) for polymer films comprising polymers at various chain lengths N and cohesion strengths ϵ_{pp}. We show the mean fields just above the grafting plane. The mean field energy per polymer (see Figure **??**) follows by the integration (over z) of $w(z)\rho(z)$, divided by the number of polymers N_p and multiplied by k_BT (see equation 13).

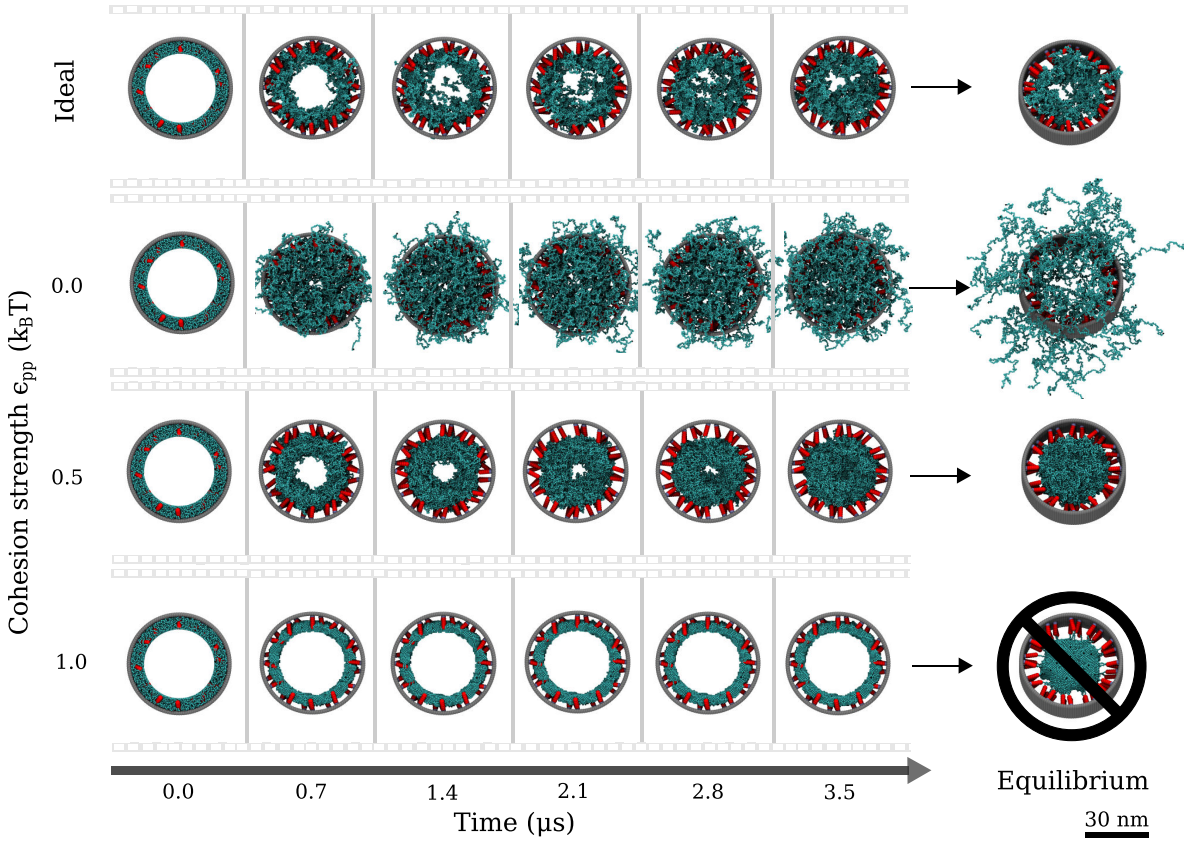

FIG. S9. Snapshots of polymer pore configurations (see Figures S5 and S6) from the dynamic resealing simulations (see Methods) and their resulting configurations after 34 μs of simulation time. For $\epsilon_{pp} = 1.0\ k_BT$ the pore did not converge to the configuration that was obtained by starting from a compact initial condition, hence the pore did not reseal.

[1] Israelachvili JN (2011) *Intermolecular and Surface Forces: Third Edition.* (Academic Press), pp. 1–676.

[2] Osmanovic D, et al. (2012) Bistable collective behavior of polymers tethered in a nanopore. *Phys. Rev. E - Stat. Nonlinear, Soft Matter Phys.* 85(6):1–8.

[3] Allen MP, Tildesley DJ (1987) *Computer Simulation of Liquids.* (Oxford University Press).

[4] Plimpton S (1995) Fast Parallel Algorithms for Short-Range Molecular Dynamics. *J. Comput. Phys.* 117(1):1–19.

[5] Mark P, Nilsson L (2001) Molecular dynamics simulations of the Ala-Pro dipeptide in water: Conformational dynamics of trans and cis isomers using different water models. *J. Phys. Chem. B* 105(33):8028–8035.

[6] Zahn R, et al. (2016) A physical model describing the interaction of nuclear transport receptors with FG nucleoporin domain assemblies. *Elife* 5:e14119.

[7] Fisher PDE, et al. (2018) A Programmable DNA Origami Platform for Organizing Intrinsically Disordered Nucleoporins within Nanopore Confinement. *ACS Nano* 12(2):1508 – 1518.

[8] Jong DHD, et al. (2011) Determining equilibrium constants for dimerization reactions from molecular dynamics simulations. *Journal of Computational Chemistry* 32(9):1919–1928.

[9] De La Torre JG, Del Rio Echenique G, Ortega A (2007) Improved calculation of rotational diffusion and intrinsic viscosity of bead models for macromolecules and nanoparticles. *J. Phys. Chem. B* 111(5):955–961.

[10] Avinery R, Kornreich M, Beck R (2018) Universal and efficient entropy estimation using a compression algorithm. *arXiv:1709.10164v3.*

[11] Seward J (2000) Bzip2 and libbzip2: A program and library for data compression.

[12] Evans R (1979) The nature of the liquid-vapour interface and other topics in the statistical mechanics of non-uniform, classical fluids. *Adv. Phys.* 28(2):143–200.

[13] Osmanović D, Ford IJ, Hoogenboom BW (2013) Model inspired by nuclear pore complex suggests possible roles for nuclear transport receptors in determining its structure. *Biophys. J.* 105(12):2781–2789.

[14] Roth R, Evans R, Lang A, Kahl G (2002) Fundamental measure theory for hard-sphere mixtures revisited: The white bear version. *J. Phys. Condens. Matter* 14(46):12063–12078.

[15] Yu YX, Wu J (2002) Density functional theory for inhomogeneous mixtures of polymeric fluids. *J. Chem. Phys.* 117(5):2368–2376.

[16] Roth R (2010) Fundamental measure theory for hard-sphere mixtures: a review. *J. Phys. Condens. Matter* 22:063102.

[17] Archer AJ, Chacko B, Evans R (2017) The standard mean-field treatment of inter-particle attraction in classical DFT is better than one might expect. *J. Chem. Phys.* 147(3):34501.

[18] Strobl G (2007) *The physics of polymers: Concepts for understanding their structures and behavior.* (Springer, Berlin).

[19] Simpson R (2004) *Proteins and Proteomics: A Laboratory Manual.* (Cold Spring Harbour Laboratory Press, U.S.), Paperback edition.

[20] Yamada J, et al. (2010) A Bimodal Distribution of Two Distinct Categories of Intrinsically Disordered Structures with Separate Functions in FG Nucleoporins. *Mol. Cell. Proteomics* 9(10):2205–2224.

[21] Wagner RS, Kapinos LE, Marshall NJ, Stewart M, Lim RYH (2015) Promiscuous binding of karyopherinβ1 modulates FG nucleoporin barrier function and expedites NTF2 transport kinetics. *Biophys. J.* 108(4):918–927.

[22] Kapinos LE, Schoch RL, Wagner RS, Schleicher KD, Lim RYH (2014) Karyopherin-centric control of nuclear pores based on molecular occupancy and kinetic analysis of multivalent binding with FG nucleoporins. *Biophys. J.* 106(8):1751–1762.

[23] Denning DP, Uversky V, Patel SS, Fink AL, Rexach M (2002) The Saccharomyces cerevisiae nucleoporin Nup2p is a natively unfolded protein. *J. Biol. Chem.* 277(36):33447–33455.